Journal of Catalysis 266 (2009) 258–267

Contents lists available at ScienceDirect

Journal of Catalysis

journal homepage: www.elsevier.com/locate/jcat

Intermolecular condensation of ethylenediamine to 1,4-diazabicyclo[2,2,2]octane over TS-1 catalysts

Yong Wang, Yueming Liu *, Xiaohong Li, Haihong Wu, Mingyuan He, Peng Wu *

Shanghai Key Laboratory of Green Chemistry and Chemical Processes, Department of Chemistry, East China Normal University, North Zhongshan Rd. 3663, Shanghai 200062, PR China

ARTICLE INFO

Article history:
Received 1 February 2009
Revised 21 May 2009
Accepted 14 June 2009
Available online 16 July 2009

Keywords:
Ethylenediamine
Triethylenediamine
Piperazine
Condensation
Titanosilicate
TS-1

ABSTRACT

The intermolecular condensation of ethylenediamine (EDA) to 1,4-diazabicyclo[2.2.2]octane or triethylenediamine (TEDA) has been carried out over various titanosilicate catalysts. Superior to Ti-MWW, Ti-Beta, Ti-FER, and Ti-MOR, TS-1 showed higher EDA conversion and TEDA selectivity. The effects of reaction parameters, Ti content, and crystal size on the EDA condensation over TS-1 have been investigated. The mechanism for the TS-1-catalyzed condensation of EDA has also been considered. The acid sites, originated from the Si–OH groups adjacent to the "open" Ti sites, were assumed to contribute to the intermolecular condensation of EDA, whereas the Lewis acid sites directly related to Ti(IV) ions were not the true active sites. The primary intermolecular condensation of EDA to 1,4-diazacyclohexane or piperazine (PIP) took place mainly inside the micropores of the MFI structure, while the secondary condensation of PIP with EDA to TEDA was favored by the acid sites located near the pore entrance and on the outer surface of crystals.

1. Introduction

1,4-Diazabicyclo[2.2.2]octane, known also as triethylenediamine (TEDA), is one of the principal catalysts used for producing polyurethanes from polyisocyanates and polyols [1]. It also acts as anti-fade reagent that scavenges the free radicals produced by excitation of fluorochromes. It is also usually added to the mounting medium in fluorescence microscopy to retard photobleaching of fluorescein and other fluorescent dyes. In addition, TEDA serves as useful structure-directing agent in zeolite synthesis [2].

The known processes for the preparation of TEDA essentially differ in the nature of the starting materials and the catalysts. Early routes to synthesize TEDA involve the vapor-phase condensation of substituted piperazines (PIP) such as aminoethylpiperazine, *N*-(2-hydroxyethyl)piperazine, and *N,N*-di(2-hydroxyethyl)piperazine over alumina catalysts [3,4], and the liquid-phase reaction in the presence of aromatic carboxylic acid catalysts [5]. Recently, the researches are reported mainly for the conversion of monoethanolamine, ethylenediamine (EDA), and PIP or their mixture over modified ZSM-5 zeolites [6–8]. The synthesis of TEDA from monoethanolamine over modified MCM-41 catalyst has also been reported [9]. In addition, the preparation of TEDA via the addition of EDA and PIP using TS-1 catalyst has been patented [10]. The previous studies disclose that the MFI type zeolites are suitable catalysts for intermolecular condensation of EDA to TEDA because of their unique shape selectivity and suitable acidic properties. Nevertheless, it is still not well addressed for the reaction mechanism on zeolites, and the parameters, particularly the nature of zeolite acidity, which determine the TEDA selectivity remain unclear.

TS-1, being able to catalyze efficiently the liquid-phase oxidation of a variety of organic compounds to oxygenated products, has brought about a breakthrough in the field of zeolite catalysis in the past two decades [11–13]. However, the application of TS-1 as an acid catalyst is seldom reported. The gas-phase Beckmann rearrangement is one of the acid-catalyzed reactions catalyzed by TS-1 [14]. In addition, TS-1 is shown to catalyze efficiently the transesterification of linear esters such as ethylacetoacetate and diethylmalonate [15].

Several studies have mentioned the acid properties of TS-1, but two different points of view have been debated for a long time [16]. Earlier study reported that TS-1 contained neither Brønsted nor Lewis acid sites [17]. On the other hand, TS-1 was inferred to be more acidic in comparison to Ti-free Silicalite-1 [18]. In addition, the significant activity given by TS-1 in the cycloaddition of CO_2 with epoxides to cyclic carbonates [19], a reaction typically catalyzed by Lewis acids such as $AlCl_3$, implies the Lewis acidity of TS-1. With respect to the Brønsted acidity of TS-1, very few reports give clear evidence for the generation of new and detectable OH groups exhibiting protic acidity after incorporating Ti in the silicalite lattice. ^{31}P and ^{1}H MAS NMR spectra of adsorbed trimethylphosphine verified that TS-1 contained also Brønsted acid sites in addition to Lewis acid sites [20], and also suggested that the incorporation of Ti into the framework led to the formation of new OH groups, titanols, which may be even more acidic than the silanols of Silicalite-1.

* Corresponding authors. Fax: +86 21 6223 2292.
E-mail addresses: ymliu@chem.ecnu.edu.cn (Y. Liu), pwu@chem.ecnu.edu.cn (P. Wu).

0021-9517/$ - see front matter © 2009 Elsevier Inc. All rights reserved.
doi:10.1016/j.jcat.2009.06.016

Because of indetermination of its acidity, it is still encouraged to carry out further study on the acidic nature of TS-1 and on how to make full use of its functions in practical acid-catalyzed reactions.

In this study, we have applied TS-1 to the intermolecular condensation of EDA to investigate its effectiveness in producing chemicals of PIP and TEDA. After comparing the catalytic performance of TS-1 with that of other titanosilicates and optimizing the reaction parameters for selective synthesis of TEDA, the active sites for the EDA conversion have been correlated to TS-1's acidity. The issue of reaction space's contributions to the consecutive condensation of EDA to PIP and finally to TEDA has also been addressed.

2. Experimental

2.1. Catalyst preparation and characterizations

TS-1 with different Si/Ti ratios was hydrothermally synthesized using tetrabutyl orthotitanate (TBOT), tetraethylorthosilicate (TEOS), and tetrapropylammonium hydroxide (TPAOH, 20% aqueous solution) by modifying the procedures reported elsewhere [21]. Typically, TEOS was mixed and stirred vigorously with a desirable amount of TBOT in a polyethylene flask at ambient temperature for 15 min. The clear solution obtained was then added dropwise to the alkali-free aqueous solution of TPAOH under stirring, which may avoid the formation of TiO_2 phase such as anatase. The mixture was stirred at room temperature for about 3 hours to hydrolyze TEOS and TBOT completely. And it was further heated at 353 K under stirring to evaporate the alcohols, resulting in the clear gels having the molar compositions of 1 SiO_2:(0.005 – 0.033) TiO_2:0.15 TPAOH:15 H_2O. The gels were charged into Teflon-lined stainless-steel autoclaves and crystallized at 443 K for 2 days under autogenous pressure and static conditions. The solid product was separated by centrifugation, washed thoroughly with distilled water, dried at 383 K overnight, and calcined in air at 823 K for 10 h to burn off the occluded organic species. For control experiment, Ti-free Silicalite-1 and other titanosilicates such as Ti-FER [22], Ti-MOR [23,24], Al-free Ti-Beta [25], and Ti-MWW [26,27] were also prepared. The TS-1 samples with larger crystal sizes were hydrothermally synthesized using fumed silica (Cab-o-sil) or colloidal silica and tetrapropylammonium bromide (TPABr) as silicon source and structure-directing agent (SDA) at Si/Ti of 60 according to the Refs. [28,29].

Sodium ion-exchanged samples were prepared by stirring 1 g of calcined TS-1 in 100 mL of 1 M $NaNO_3$ or 1 M Na_2CO_3 solution at room temperature for 24 h. And the removal of sodium ions was carried out by washing with 1 M HNO_3 solution at room temperature.

All of the catalysts were characterized by inductively coupled plasma (ICP) on a Thermo IRIS Intrepid II XSP atomic emission spectrometer, X-ray diffraction (XRD) on a Bruker D8 ADVANCE diffractometer (Cu-Kα), N_2 adsorption on an Autosorb Quancachrome (02108-KR-1), scanning electron microscopy (SEM) on a JEOL JSM-T220 (Hitachi S-4800), and UV–visible (Shimadzu UV-2400PC) and IR (Nicolet NEXUS-FTIR-670) spectroscopies. The amount of sodium was determined by atomic adsorption spectroscopy (AAS). IR spectra of pyridine adsorption were recorded as follows: a self-supported wafer (9.6 mg cm^{-2} thickness and $\varnothing$ 2 cm) was set in a quartz IR cell sealed with CaF_2 windows, where it was evacuated at 773 K for 2 h before the pyridine adsorption. The adsorption was carried out by exposing the wafer to a pyridine vapor (1.3 kPa) at 323 K for 0.5 h. The physisorbed pyridine was then removed by evacuation at different temperatures (323–470 K) for 1 h. All the spectra were collected at room temperature.

2.2. Catalytic reactions

The intermolecular condensation of EDA was carried out in a down-flow fixed-bed reactor at atmospheric pressure. In a typical run, 1 g of catalyst (18–30 mesh size) was activated at 673 K for 3 h in a flow of N_2. After cooling to the reaction temperature, the reaction was started by feeding an aqueous EDA solution (50 wt% EDA in H_2O) into the reactor at a flow rate of 5 mL h^{-1} together with a nitrogen flow of 30 mL min^{-1}. The products were collected in a receiver cooled with an ice-salt bath. The amounts of the products were quantified on a Shimadzu 14B gas chromatograph equipped with an OV-1 column (30 m) and an FID detector, and they were identified using authentic samples or by GC–MS (Agilent 6890).

3. Results

3.1. Characterization of various titanosilicate catalysts

All titanosilicates had objective zeolite structures and relatively high crystallinity, and contained no impurity of other zeolite phase as detected by XRD patterns (Fig. 1). In UV–visible and IR spectra, the samples showed the characteristic adsorption bands at 210 nm and 960 cm^{-1}, respectively, which are assigned to the tetrahedral Ti species isolated in the zeolite framework [11,12,26]. These titanosilicates had reasonably high surface area (Langmuir) in the range of 430–653 m^2 g^{-1} as determined by N_2 adsorption (Table 1).

The TS-1 samples synthesized using TEOS and TPAOH at various Si/Ti ratios were further characterized. The samples contained essentially the isolated Ti species in the framework as evidenced by the predominant band at 210 nm in UV–visible spectra when the Si/Ti ratio was higher than 60 (Fig. 2a–d). Nevertheless, the band due to the anatase-like Ti species, although not intense, was also observed in addition to the 210-nm band for the samples synthesized at Si/Ti ratios of 40 and 30 (Fig. 2e and f), which is indicative of the presence of a small amount of extraframework Ti. The IR spectra of TS-1 in the framework vibration region showed the characteristic band at 960 cm^{-1} assigned to the framework Ti, and the band intensity increased with increasing Ti content (not shown). Thus, both IR and UV–visible spectra verified that the TS-1 catalysts were of good quality in terms of incorporating the tetrahedrally

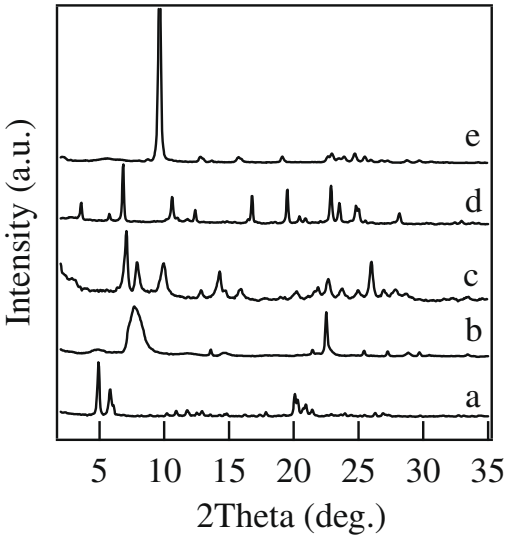

Fig. 1. Representative XRD patterns of TS-1 (60) (a), Ti-Beta (37) (b), Ti-MWW (55) (c), Ti-MOR (90) (d), and Ti-FER (52) (e). The number in the parentheses represents the Si/Ti molar ratio.

Table 1
The result of intermolecular condensation of EDA over different titanosilicate catalysts.[a]

No.	Catalyst	Si/Ti[b] ratio	SA[c] ($m^2\ g^{-1}$)	Main pores	EDA conv. (%)	Product sel. (%)		
						PIP	TEDA	Others[d]
1	TS-1	60	530	3D 10-MR	84.4	31	51	18
2	Ti-Beta	37	653	2D 12-MR	41.1	45	15	40
3[e]	Ti-Beta	37	653	2D 12-MR	80.5	10	45	45
4	Ti-MOR	90	553	1D 12-MR	30.5	48	18	34
5	Ti-MWW	55	610	2D 10-MR (12-MR cup, supercage)	35.0	58	7	35
6	Ti-FER	52	430	1D 10-MR	25.0	43	37	20

[a] Reaction conditions: catalyst, 1 g; pressure, 1 atm; temp.: 623 K; EDA feed (50 wt% aqueous solution), 5 mL h^{-1}; N_2, 30 mL min^{-1}; TOS: 3 h.
[b] Given by ICP.
[c] Specific surface area (Langmuir) given by N_2 adsorption at 77 K.
[d] Mainly lower aliphatic amines and the derivatives of pyrazine.
[e] Reaction conditions: N_2, 10 mL min^{-1}; others, same as a.

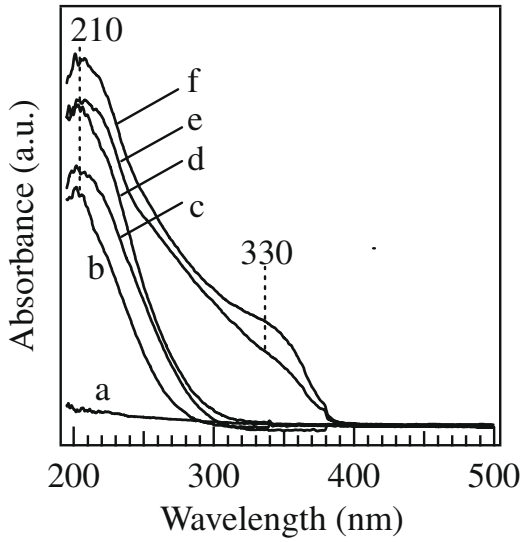

Fig. 2. UV–visible spectra of TS-1 synthesized at Si/Ti ratio of ∞ (a), 200 (b), 100 (c), 60 (d), 40 (e), and 30 (f).

coordinated Ti ions. The scanning electron microscopy (SEM) revealed that TS-1 was composed of 300–400 nm spherical crystals, the size of which was independent of the Ti content (Fig. 3a and b). On the other hand, TS-1 with larger crystals was synthesized when using other silicon source or SDA. The TS-1 sample obtained from fumed silica and TPAOH consisted of the spherical crystals of ca. 20 μm (Fig. 3c), while the sample prepared using colloidal silica and TPABr as SDA showed a morphology of 30 × 8 × 2 μm plate crystals (Fig. 3d). Nevertheless, UV–visible spectra showed that both large crystal samples contained the isolated tetrahedral Ti specie but no anatase phase.

On the basis of the crystallinity, surface area, and the nature of Ti species, these titanosilicates qualified as the catalysts for intermolecular condensation of EDA.

3.2. Intermolecular condensation of EDA over various titanosilicates

According to the mechanism reported previously [6] and the products actually obtained, a general reaction pathway showing the product distribution of intermolecular condensation of EDA was obtained (Scheme 1). The major products were PIP and TEDA,

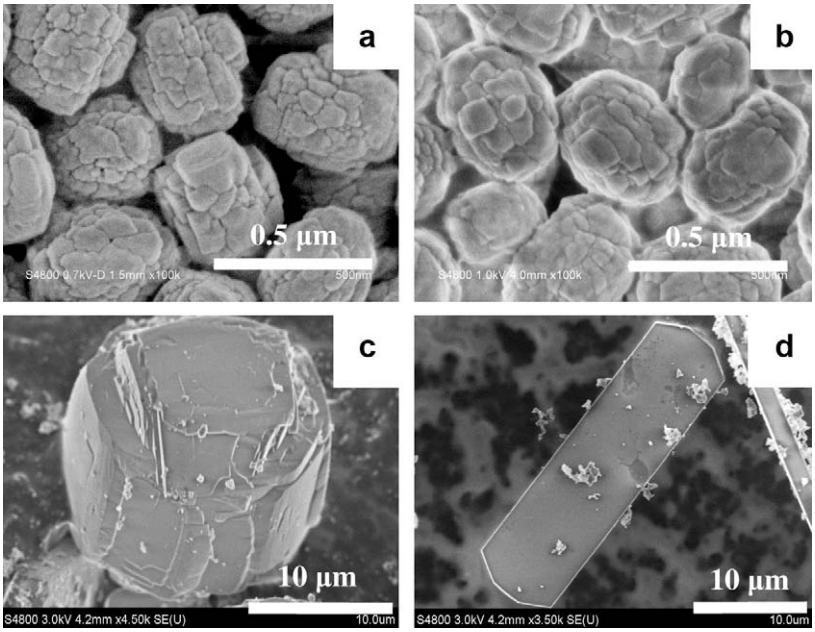

Fig. 3. SEM images of TS-1 samples synthesized with TEOS and TPAOH at Si/Ti of 60 (a), 40 (b), synthesized with fumed silica and TPAOH (c), and with silica sol and TPABr (d) both at Si/Ti of 60.

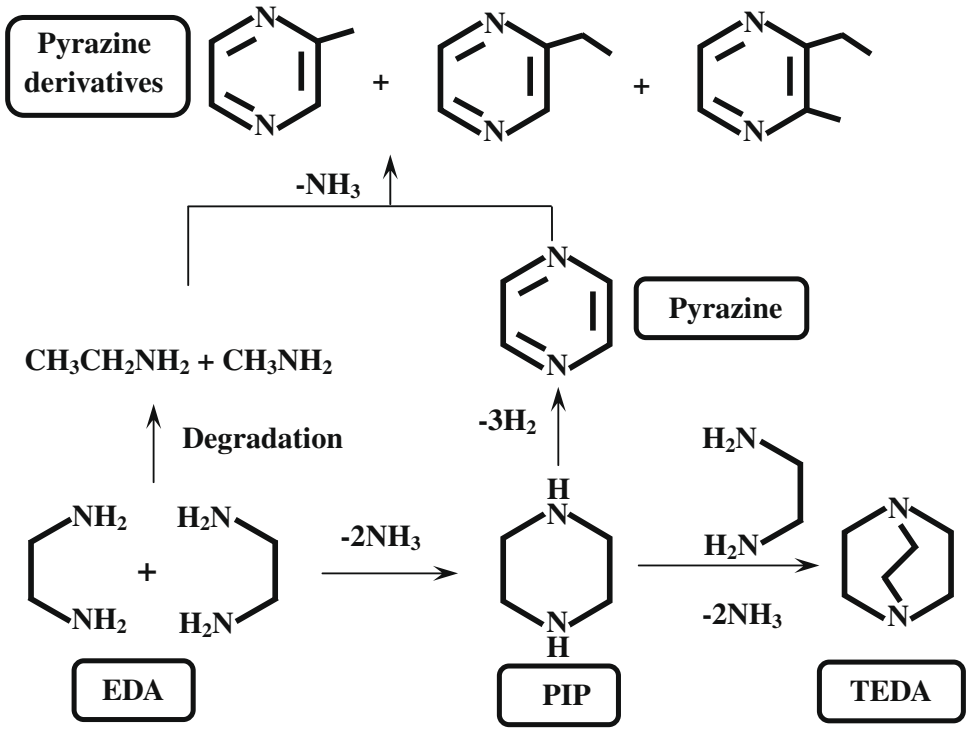

Scheme 1.

while the byproducts were lower aliphatic amines (ethylamine and methylamine) and the derivatives of pyrazine. Intermolecular deamino-condensation of two EDA molecules led to the formation of PIP, which further condensed with one more EDA molecule to give TEDA. Meanwhile, PIP partially underwent dehydrogenation to form pyrazine that may further react with the products from EDA degradation to produce the corresponding derivatives, alkyl pyrazines.

Table 1 shows the comparison of the results of intermolecular condensation of EDA among various titanosilicate catalysts. The products were mainly PIP and TEDA together with some lower aliphatic amines and the pyrazine derivatives. The EDA conversion and product selectivity remained almost unchangeable during 10 h of time on stream (TOS) investigated. Under optimized conditions (the details will be given in later sections), TS-1 showed the highest EDA conversion and more importantly, the highest total selectivity to PIP and TEDA (Table 1, No. 1). Other titanosilicates were not only less active, but also less selective to PIP and TEDA even when compared at equal conversion (Table 1, Nos. 2–6). Therefore, the catalytic properties of TS-1 were then further studied by investigating the effects of various reaction parameters.

3.3. Effects of reaction parameters on the intermolecular condensation of EDA over TS-1

3.3.1. Effect of reaction temperature

The reaction temperature exhibited a great effect on the intermolecular condensation of EDA over TS-1(60). As shown in Fig. 4, the conversion of EDA increased with increasing temperature, whereas the selectivity to PIP decreased monotonously and the TEDA selectivity increased first and then decreased slightly. The TEDA selectivity reached a maximum value of 51% at 623 K, where the EDA conversion and the PIP selectivity were 84% and 31%, respectively. When the temperature was further raised to 673 K, EDA was 100% converted, whereas PIP showed an exponential decrease in selectivity to nearly zero, and the formation of byproducts was enhanced obviously. At high temperatures, the Lewis acidic sites may be formed due to the dehydroxylation, which then contributes to the formation of pyrazine derivatives [30]. Moreover, the experiment indicated that the degradation of EDA to the aliphatic amines occurs more easily at higher temperatures. This may also make the selectivity to PIP and TEDA decrease. The reaction at the temperatures below 623 K does not favor the formation of pyrazine and its derivatives, but is suitable for the formation of the main products of PIP and TEDA [7]. However, too low

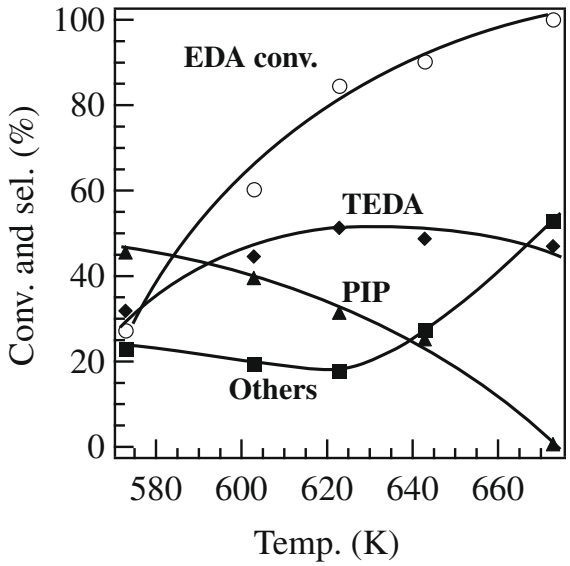

Fig. 4. Effect of reaction temperature on the intermolecular condensation of EDA on TS-1 (Si/Ti = 60). Other reaction conditions: see Table 1.

temperatures are energetically inefficient for converting EDA to PIP and further to TEDA. Consequently, the foregoing experiments showed that the intermolecular condensation of EDA to TEDA proceeded most effectively at an optimum reaction temperature of 623 K at catalyst loading of 1 g, EDA feeding rate of 5 mL h^{-1} and N_2 flow rate of 30 mL min^{-1}.

3.3.2. Effect of concentration of EDA

Fig. 5 shows the effect of the concentration of EDA on the reaction at 623 K. TS-1 showed the highest EDA conversion at 10 wt% of aqueous EDA. The conversion was comparably high in the range of 20–90% concentration, but the product selectivity varied greatly. At 50% concentration of EDA, the catalyst gave the highest selectivity to TEDA (51%) as well as the highest total selectivity to PIP and TEDA (82%). Lowering the EDA concentration, the selectivity of PIP and TEDA decreased greatly owing to the formation of byproducts. At higher concentration of EDA, the conversion of EDA was still higher than 80%, the TEDA selectivity decreased, and the catalyst turned to deactivate at 3 h of TOS. Meanwhile, the effluent became very thick because of high concentration of heavy products having high boiling points, and the catalyst deactivated more rapidly. Steam is assumed to have the function of refreshing the catalytic active sites by washing out the basic product molecules adsorbed strongly on the acid sites inside zeolite channels or on crystal surface. This is then helpful for reducing the coke formation. Thus, a moderate concentration of EDA is preferable to achieve a high EDA conversion and high selectivity to PIP and TEDA.

3.3.3. Effect of contact time

The contact time expressed as catalyst weight to flow (W/F) ratio was varied in a wide range to determine what were the primary products in the intermolecular condensation of EDA (Fig. 6). The reactions were carried out by varying the catalyst amount at 623 K with an EDA (50 wt%) feed rate of 5 mL h^{-1}. The conversion of EDA and selectivity to TEDA increased with increasing W/F ratio, while the selectivity to PIP decreased. Apparently, the intermolecular condensation of EDA was a typical consecutive reaction, namely, PIP was primarily produced immediately after the contact of reactant molecules with the catalyst bed, and it was successively converted to TEDA as a result of secondary condensation with EDA in deep catalyst bed. Meanwhile, a long contact time made the side reactions take place easily, leading to a high selectivity for byproducts such as lower aliphatic amines and pyrazine derivatives.

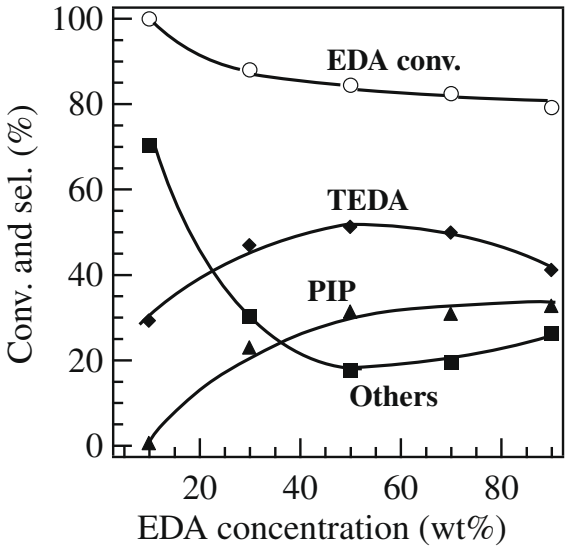

Fig. 5. Effect of concentration of EDA on the intermolecular condensation of EDA on TS-1 (Si/Ti = 60). Reaction conditions: see Table 1.

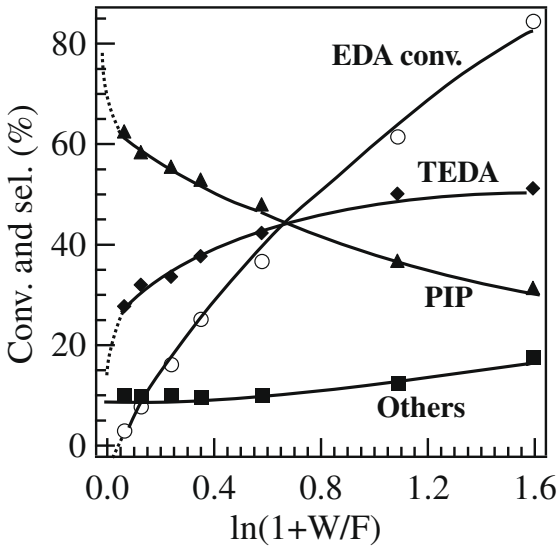

Fig. 6. Effect of contact time on the intermolecular condensation of EDA on TS-1 (Si/Ti = 60). Other reaction conditions: see in Table 1.

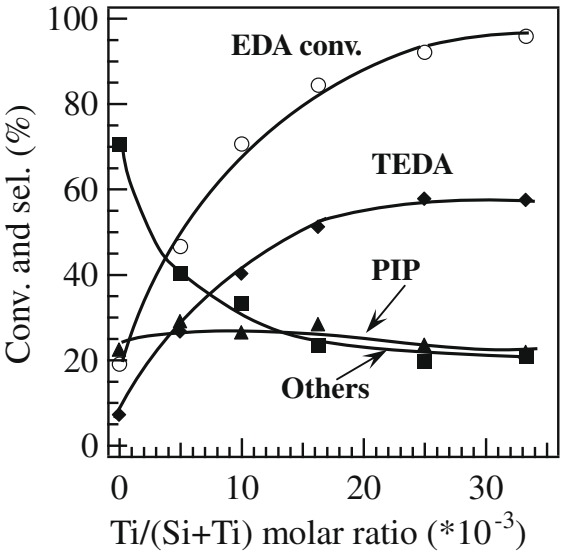

Fig. 7. Dependence of EDA conversion and product selectivity on the Ti content of TS-1. Other reaction conditions: see Table 1.

3.3.4. Effect of Ti content

A series of TS-1 catalysts with Si/Ti ratios of 30–200 were prepared, and applied to the intermolecular condensation of EDA together with Silicalite-1 (Fig. 7). Silicalite-1 free of Ti but containing silanol groups was not active and selective to the reaction, giving only 19.5% EDA conversion and 7.5% TEDA selectivity. Both the EDA conversion and TEDA selectivity increased reasonably with increasing Ti content, but reached a ceiling at a Ti content of 0.25 mmol g^{-1} (corresponding to Si/Ti = 40). This is probably due to the presence of a part of anatase phase in the high Ti content samples as evidenced by UV–visible spectra (Fig. 2).

4. Discussion

4.1. The effect of zeolite structure on the EDA conversion

Table 1 shows that the catalytic performance depended greatly on the titanosilicates. Except for Ti-MOR, the titanosilicates

employed in the reaction had comparable Si/Ti ratio. The Ti content is thus presumed not to account for the greatly different catalytic properties observed between TS-1 and the other catalysts. The advantage of TS-1 must originate from the medium porosity of 10-MR windows and the unique hydrophobic nature of the MFI topology. These results are fully consistent with the findings observed on the aluminosilicate zeolites, among which modified ZSM-5 was reported to be the most shape-selective and effective catalyst for the conversion of PIP to TEDA [8].

In the case of Ti-Beta and Ti-MOR, the selectivity to TEDA decreased, while the alkylpyrazine byproducts were more coproduced. This is because the 12-MR large pores of the *BEA and MOR topologies are not narrow enough to suppress the alkylation of pyrazine to the corresponding derivatives with large molecular sizes (Table 1, Nos. 2 and 4). Ti-Beta, containing a large quantity of stacking faults related to its polymorphic crystalline structure and then exhibiting a highly hydrophilic feature, reasonably showed a lower EDA conversion with the reaction operated under steaming conditions. The low activity of Ti-MOR is considered to be related to its one-dimensional 12-MR channels not suitable for the diffusion and desorption of bulky molecules such as TEDA. Hence, both Ti-MOR and Ti-Beta were not active and selective for the synthesis of TEDA. Ti-FER imposed more significant diffusion limitation for the product molecules practically because of its one-dimensional 10-MR channels with an elliptical shape and smaller window than that of MFI, and then showed the lowest conversion (Table 1, No. 6). In addition, Ti-MWW was composed of two independent interlayer and intralayer 10-MR channels both of which are two-dimensional but slightly smaller than that of TS-1. The pore entrance of the MWW structure may impose a serious steric hindrance to the cyclic products, which made Ti-MWW less active than TS-1 (Table 1, No. 5). Moreover, the open reaction spaces of the MWW structure, namely, the 12-MR side cups on the exterior surface and the 12-MR supercages embedded in interlayer 10-MR channels, made Ti-MWW less shape-selective either. Above results indicated that only TS-1 with the MFI topology and medium porosity is possible to give an outstanding catalytic activity and TEDA selectivity not shared by the other zeolite structure in the intermolecular condensation of EDA.

4.2. Investigation into the active sites for EDA condensation on TS-1

Fig. 7 shows that the EDA conversion and the TEDA selectivity depended closely on the Ti content of TS-1. The results implied that the catalytic active sites for the EDA condensation to TEDA related to the framework Ti species. In solid acid-catalyzed reactions, the framework Ti species of TS-1 can serve as Lewis acid sites. For instance, TS-1 shows a significant activity for the cycloaddition of CO_2 to epoxides to give cyclic carbonates [19]. On the other hand, the neural, moderately acidic, isolated surface silanol groups are reported to be responsible for the gas-phase Beckmann arrangement of cyclohexanone oxime [14].

IR spectroscopy has been adopted to investigate the acidity of TS-1. Fig. 8 shows the IR spectra in the region of hydroxyl stretching vibration of TS-1 and Silicalite-1 after dehydration at 773 K. Silicalite-1 showed a sharp band at 3725 cm^{-1} together with a broad one at 3500 cm^{-1} (Fig. 8a), which are attributed to the location of terminal silanol internal to zeolite pores and the hydrogen-bonded silanol nests, respectively [31], suggesting the presence of a relatively high concentration of defect sites in Silicalite-1. With increasing Ti content, the TS-1 samples showed a progressive decrease in the intensity of the broad band which simultaneously shifted from 3505 to 3520 cm^{-1}. The main band in the left side, on the other hand, gradually became sharper and projected at 3741 cm^{-1} when the Si/Ti ratio was below 60. The 3741 cm^{-1} band is attributed to the terminal silanol on the external surface of zeolite crystals. The observed behavior is in agreement with previous studies which report that Silicalite-1 contains many structural defects while the incorporation of tetrahedral Ti ions tends to mend these defects to reduce their number [32]. In addition, the 3676 cm^{-1} band, once ascribed to the titanol groups [33], was not distinctive probably because the stretching of Ti–OH group was far less intense than silanol groups, or its vibration mode did not give a sharp enough band to be observable.

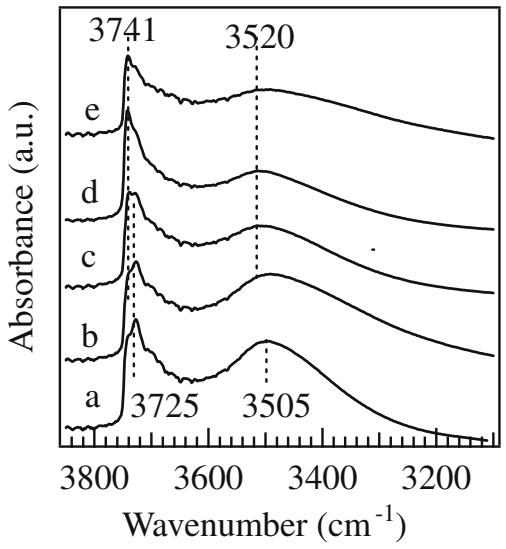

Fig. 8. IR spectra in hydroxyl stretching region of dehydrated TS-1 synthesized at Si/Ti ratio of ∞ (a), 200 (b), 60 (c), 40 (d), and 30 (e).

Pyridine was then used as a probe molecule to provide more detailed informations of acid site's types, strength, and amount. Fig. 9 shows the IR spectra of adsorbed pyridine in the range of pyridine ring-stretching modes after desorption at various temperatures. Since the pyridine adsorption did not cause apparent change in the region of hydroxyl stretching vibration, the corresponding spectra thus are not shown for concision. As shown in Fig. 9A, Silicalite-1 showed the vibrations of stretching modes of hydrogen-bonded (hb) and physically (ph) adsorbed pyridine at 1599 cm^{-1} (hb, mode 8a), 1589 cm^{-1} (ph, mode 8a), 1581 cm^{-1} (hb, ph, mode 8 b), 1483 cm^{-1} (hb, mode 19a), 1446 cm^{-1} (hb, mode 19b), and 1440 cm^{-1} (ph, mode 19b) [34–36]. The bands at 1589, 1483, and 1440 cm^{-1} associated with physically adsorbed pyridine nearly diminished after desorption at 323 K. The bands at 1599 and 1446 cm^{-1} associated with hydrogen-bonded pyridine were more resistant against evacuation, but decreased in intensity with rising desorption temperature, and disappeared totally at 473 K. Thus, the acidity related to the silanols in Silicalite-1 was not strong. On the other hand, the band at 1490 cm^{-1} characteristic of both Brønsted and Lewis acids was absent in the spectra of Silicalite-1 regardless of desorption temperature, suggesting it was almost free of Lewis acid sites.

In the spectra of TS-1 (Fig. 9B), we observed two distinct bands at 1604 and 1490 cm^{-1} and a shoulder one at 1450 cm^{-1} (superimposed to those of hydrogen-bonded pyridine) in addition to similar bands shown by Silicalite-1. These new components absent for Silicalite-1 were more evacuation temperature resistant, and remained even after desorption at 473 K. The bands at 1604 and 1490 cm^{-1}, apparently related to the Ti species incorporated into the matrix of silicalite, are assigned to the pyridine-ring vibration modes of 8a and 19a, respectively [36,37]. The $C_5H_5N\cdots Ti(IV)$ adduct with pyridine molecule (ligand) coordinated to the Ti(IV) ion (center) may contribute to these bands. These two bands can be taken as the evidence for the presence of Lewis acid sites with

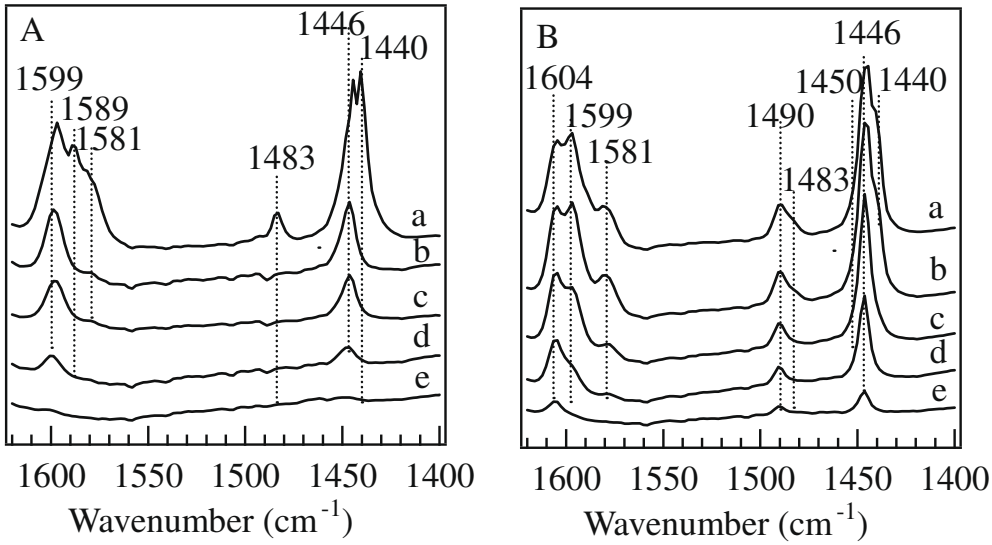

Fig. 9. IR spectra of Silicalite-1 (Si/Ti = ∞) (A) and TS-1 (Si/Ti = 40) (B) after pyridine adsorption without evacuation (a), and after evacuation at 323 K (b), 373 K (c), 423 K (d), and 473 K (e) for 1 h, respectively.

a relatively high strength in TS-1. The spectra did not show an obvious band at 1550 cm^{-1} which is assigned to the vibration of pyridium ion formed by protonation of pyridine ring, and commonly used as an evidence for the presence of Brønsted acid sites. Nevertheless, the 1446 cm^{-1} band due to hydrogen-bonded pyridine was still visible after desorption at 473 K (Fig. 9B, e). TS-1 is thus presumed to possess relatively stronger acid sites than Silicalite-1. These acid sites are related to the hydroxyl groups adjacent to the framework Ti.

Pyridine adsorption was further carried out on the TS-1 samples with various Ti contents. Fig. 10 shows the comparison of the spectra of the samples after removing weakly adsorbed species by evacuation at 473 K. The bands at 1604, 1490, and 1446 cm^{-1}, absent for Silicalite-1, increased in intensity with increasing Ti content. Thus, the introduction of tetrahedrally coordinated Ti created in TS-1 the Lewis acid sites that exhibited the former two bands ascribed to coordinated pyridine species (the contribution to the 1490 cm^{-1} band of the pyridium ions generated from

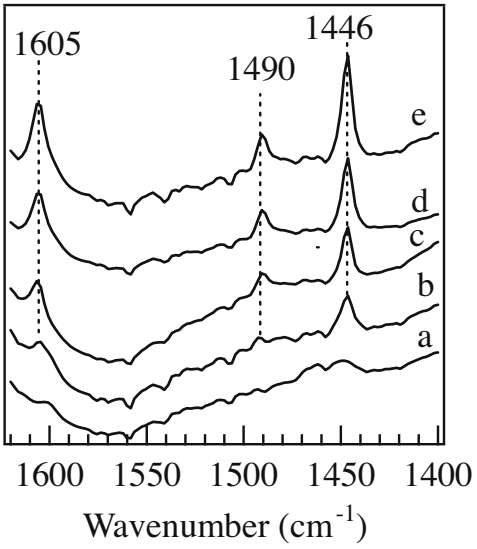

Fig. 10. Pyridine-adsorbed IR spectra after evacuation at 473 K for 1 h of TS-1 synthesized at Si/Ti ratio of ∞ (a), 200 (b), 60 (c), 40 (d), and 30 (e).

chemisorbed pyridine on Brønsted acid sites would be negligible for weak solid acid of TS-1), and also developed the hydroxyl groups showing the latter one due to hydrogen-bonded species. It is deduced that the TS-1 catalysts contained somewhat strong Lewis acid sites and hydroxyl groups with a moderate acidity (at least tolerant to the pyridine desorption at 473 K), whereas Silicalite-1 contained only the neutral silanols.

The above results are in agreement to the characterizations and catalysis reported for TS-1. Silanols as well as titanols possibly present in TS-1 are reported to act potentially as weak acid sites [38]. ^{31}P MAS NMR spectroscopy using trimethylphosphine as basic probe molecule showed that the amount of acid sites of TS-1 increased with increasing Ti content [39]. Therefore, TS-1 is an active and selective catalyst for the gas-phase Beckmann rearrangement of cyclohexanone oxime, a reaction believed to take place on the hydroxyl groups of zeolites [14]. In addition, the framework Ti(IV) ions in the vicinity of the silanol groups could change the electron density around Si owing to different electronegativity of Ti to Si, or due to a local structure deformation caused by the introduction of bulky Ti ions into the framework. The strength of the SiO–H bond then may become weakened, making it donate the proton easily. This is presumed to be one of the possibilities that TS-1 shows a relatively stronger acidity than Silicalite-1 [40,41].

In order to differ the active sites between the acidity relative to hydroxyl groups and Lewis acidity for the intermolecular condensation of EDA on TS-1, we have carried out the removal of hydroxyl-related active sites with Na^+ ion-exchange and the regeneration of acidity by acid retreatment, and investigated the effect of these post treatments on the catalytic activity. The alkali cations incorporated by either direct hydrothermal synthesis or post ion-exchange are shown to poison the active sites of TS-1 [42]. As shown in Scheme 2, the Na^+ ion-exchange occurred mainly on the Si–OH group adjacent to the "open" Ti site but not on the SiOH···HOSi sites or the isolated terminal SiOH sites. Since the isoelectric points of SiO_2 and TiO_2 are in the pH range of 2–3, and 5–6, respectively, the SiO–H groups should be more easily ion-exchanged than the TiO–H groups.

Fig. 11 shows the IR spectra in the structure vibration region of TS-1 before and after various ion-exchanges. When TS-1 was exchanged with $NaNO_3$ solution, the characteristic band at 963 cm^{-1} due to the framework Ti ions remained almost intact (Fig. 11a and b). However, the 963-cm^{-1} band disappeared completely and

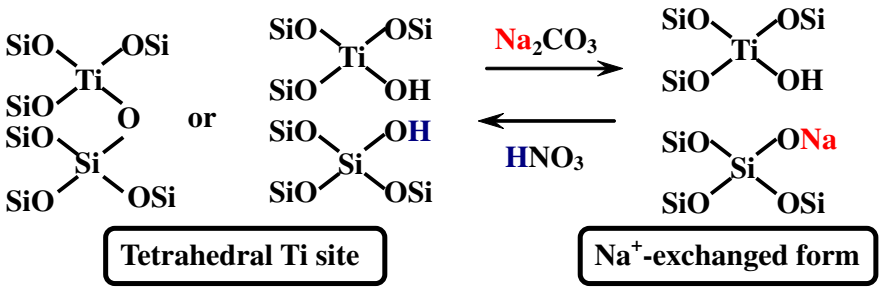

Scheme 2.

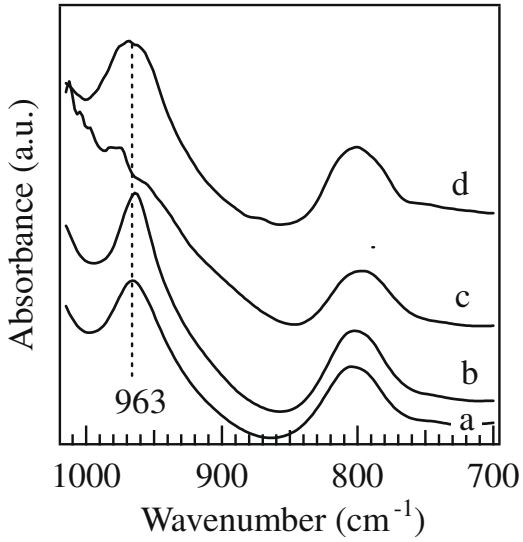

Fig. 11. IR spectra in framework vibration region of TS-1 (Si/Ti = 40) (a), (a) treated with $NaNO_3$ (b), (a) treated with Na_2CO_3 (c), and (c) washed with HNO_3 (d).

turned to a shoulder at 985 cm^{-1} when the sample was ion-exchanged in a more basic solution of Na_2CO_3 (Fig. 10c). A subsequent washing of Na–TS-1 with 1 M HNO_3 solution at room temperature restored the 963-cm^{-1} band (Fig. 11d), the slight broadness of which suggested that the sample adsorbed a large number of water molecules on the defect sites developed by desilication, since we observed that the sample lost weight by 25 wt% after Na_2CO_3 treatment.

The Na content analyses indicate that the ion-exchange with $NaNO_3$ incorporated a relatively low amount of sodium into TS-1, while the exchange with Na_2CO_3 resulted in a much higher Na content than that of Ti (Table 2, Nos. 1, 2 and 4). In agreement to previous observations [21,42], the results indicate that the exchange of sodium for the protons in TS-1 takes place more readily at high pH. The sodium ions were removed to a very low level after a further washing with 1 M HNO_3 at room temperature for 24 h, whereas the Ti content was influenced rarely (Nos. 3 and 5). The Na^+ ion-exchanged and further acid-treated samples showed very similar UV–visible spectra to the parent TS-1 (see Supporting information, Fig. S1). All samples contained mainly the isolated Ti species in the framework since the 220-nm band was the predominant adsorption band in their UV spectra. These indicate that the state of Ti species was intact by these treatments.

Table 2 lists also the catalytic activity of the ion-exchanged TS-1 samples for intermolecular condensation of EDA. Compared with the parent TS-1, the sample exchanged with $NaNO_3$ decreased slightly in EDA conversion, and showed very similar EDTA selectivity but a lower selectivity for byproducts. The removal of sodium by subsequent acid washing recovered the activity and the product selectivities (Nos. 1–3) almost totally. However, the ion-exchange with Na_2CO_3 caused the EDA conversion to decrease dramatically from 92.1% to 6.5% (No. 4). The acid washing with HNO_3 recovered the catalytic performance greatly (No. 5). The incomplete regeneration may be due to an insufficient removal of the poisoning sodium ions.

Fig. 12A shows the IR spectra of TS-1 before and after ion-exchange in the region of hydroxyl stretching vibration. Compared with the parent sample, the bands at 3741 and 3725 cm^{-1} varied little when exchanged with $NaNO_3$, whereas the 3505-cm^{-1} band, ascribed to hydrogen-bonded silanol groups probably on internal defect sites such as hydroxyl nests, decreased in intensity apparently (Fig. 12A, a and b). These hydroxyl groups were regenerated after acid treatment (Fig. 12A, c). On the other hand, the ion-exchange with Na_2CO_3 removed various OH groups significantly, leading to a spectrum consisting of only a weak band at

Table 2
The results of intermolecular condensation of EDA over the TS-1 catalysts after various post-treatments.[a]

No.	Catalyst	Si/Ti[b]	Na_2O[c] (wt%)	Na/Ti ratio	EDA conv. (%)	Product sel. (%)		
						PIP	TEDA	Others[d]
1	TS-1	39	Trace	–	92.1	24	58	18
2	TS-1-$NaNO_3$[e]	40	0.77	0.60	76.7	29	62	9
3	TS-1-Na_2CO_3-AW[f]	40	0.08	0.06	88.5	27	60	13
4	TS-1-Na_2CO_3[e]	36	4.05	2.82	6.5	42	40	18
5	TS-1-Na_2CO_3-AW[f]	41	0.18	0.14	81.7	24	53	23

[a] Reaction conditions: see Table 1.
[b] Determined by ICP.
[c] Determined by AAS.
[d] Mainly lower aliphatic amines and the derivatives of pyrazine.
[e] The ion-exchange was carried out in 1 M $NaNO_3$ or Na_2CO_3 solution at room temperature, respectively.
[f] AW, acid washing with 1 M HNO_3 at room temperature.

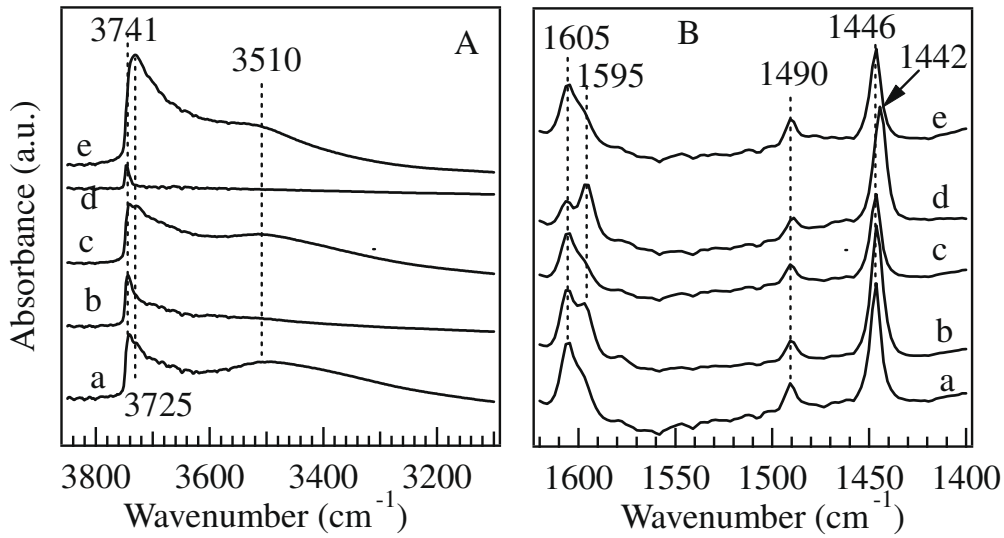

Fig. 12. IR spectra of TS-1 (Si/Ti = 40) before (A) and after pyridine adsorption (B). (a) Parent; (b) as a after $NaNO_3$ treatment; (c) as b after HNO_3 washing; (d) as a after Na_2CO_3 treatment, and (e) as d after HNO_3 washing (e). The pyridine desorption was carried out by evacuation at 423 K for 1 h.

3741 cm^{-1} due to terminal silanols (Fig. 12A, d). The acid washing then regenerated the hydroxyl groups by removing the counterpart sodium ions (Fig. 12A, e). Thus, the hydroxyl groups-related acidity in TS-1 depends greatly on the form of ion-exchange.

The sodium ion-exchange developed two additional bands at 1592 and 1442 cm^{-1} in pyridine-adsorbed IR spectra in comparison to the parent TS-1 (Fig. 12B). The phenomena were particularly obvious in the case of extensively ion-exchanged sample with Na_2CO_3 solution (Fig. 12B, d). These two bands (mode 8a and 19b of the pyridine ring) are attributed to pyridine adsorbed on alkali ions [43–45]. The still existence of the bands at 1605 and 1490 cm^{-1} implies that the sodium ion-exchange did not replace all the protons in TS-1, although it removed most hydroxyl groups. The removal of sodium ions by acid washing made the local chemical environment around the Ti site reversible to go back to its original state (Scheme 2), and then the spectra of adsorbed pyridine turned to be the same as the parent TS-1 (Fig. 12B, c and e). In particular, the band at 1442 cm^{-1} changed back to the hydrogen-bonded one at 1446 cm^{-1}. These results would deny the contribution to the EDA conversion of the Lewis acidity directly related to the framework Ti ions in TS-1, but support that the actual active sites for intermolecular condensation of EDA are those Si–OH groups adjacent to the so-called "open" Ti sites, which show a moderate acidity as evidenced by the hydroxyl stretching vibration as well as the hydrogen-bonded pyridine vibration at 1446 cm^{-1}.

4.3. Investigation into the reaction spaces of TS-1 for EDA condensation

The reports reported so far deal rarely with the issue of reaction spaces for the intermolecular condensation of EDA which involves the reaction steps of small reactant molecules to monocyclic intermediate and further to more bulky multicyclic product. The TS-1 samples with varying crystal sizes were thus synthesized using different silicon and SDA sources to investigate the contribution of intracrystal channels and the outer surface to the reaction (Table 3). The catalytic properties were strongly influenced by the size of the crystals of TS-1. When the TS-1 samples with similar spherical morphology increased in crystal size from an average size of 0.3–20 μm, the EDA conversion decreased from 84.4% to 79.5% (Nos. 1 and 2). At similar EDA conversion, the selectivity to TEDA dropped from 53% to 39% (No. 3). On the other hand, the plate-shaped TS-1 zeolite with a much larger crystal size of 30 × 8 × 2 μm gave the lowest EDA conversion (No. 4), and the lowest selectivity to TEDA even at similar EDA conversion (No. 5). The orientation of the pore system is presumed to affect the diffusion rate of the molecules for this catalyst which had greatly different crystal lengths or widths on three crystal faces. The zigzag 10-MR channels (0.51 × 0.55 nm) with a relatively smaller pore size are parallel to the plate crystals. They are considered to provide a longer diffusion pathway for the molecules than the straight 10-MR channels (0.53 × 0.56 nm) perpendicular to the plate crystal (the thinnest

Table 3
The result of intermolecular condensation of EDA over TS-1 catalysts with various crystal size.[a]

No.	Si/Ti ratio[b]	Crystal[c]		EDA conv. (%)	Product sel. (%)		
		Size (μm)	Morphology		PIP	TEDA	Others[d]
1	60	0.3–0.4	spherical	84.4	31	53	16
2	61	20	spherical	79.5	52	32	16
3[e]	61	20	spherical	84.0	41	39	20
4	58	30 × 8 × 2	plate shaped	71.1	64	21	15
5[e]	58	30 × 8 × 2	plate shaped	82.1	51	28	21

[a] Reaction conditions: see Table 1.
[b] Determined by ICP.
[c] Determined by SEM.
[d] Mainly lower aliphatic amines and the derivatives of pyrazine.
[e] Reaction conditions: N_2, 10 mL min^{-1}.

direction), and then make the molecules suffer more diffusion limitations. This may correspond to the lowest EDA conversion as well as the lowest selectivity to bulky product of TEDA on this TS-1 with a large crystal size. It is thus favorable to reduce the crystal size and then increase the external surface area to make the primary condensation of EDA to PIP and the secondary condensation of PIP to TEDA both moving smoothly. The average molecular sizes are 0.31×0.54 nm for EDA, 0.27×0.48 nm for PIP and $0.46 \times 0.48 \times 0.48$ nm for TEDA as given by Gaussian2003 software. Therefore, we assume that the first intermolecular condensation of EDA to PIP takes place mainly inside the medium pores of the MFI structure. With respect to secondary condensation of PIP with EDA to TEDA, since the TEDA molecules with a polycyclic shape are relatively rigid, the 10-MR channels of TS-1 would propose mass transfer limitations inside for these molecules. Moreover, TEDA is formed via a bulky intermediate of aminoethylpiperazine ($0.27 \times 0.48 \times 0.7$ nm), which is hardly accommodated inside the pores of the MFI structure. Thus, the condensation of PIP with EDA is considered to take place mainly on the acid sites near the pore entrance and on the external surface.

5. Conclusions

TS-1 is superior to other titanosilicates in the intermolecular condensation of EDA to TEDA, giving EDA conversion to PIP and TEDA as high as 95% and a total selectivity of ca. 85%, when synthesized to have small a crystal size (0.3–0.4 μm) as well as a high Ti content corresponding to Si/Ti ratio of 30. The incorporation of Ti ions into the framework generates both acidic hydroxyl groups and Lewis acid sites in TS-1. The acidic hydroxyl groups with a moderate acidity is originated from the internal Si–OH groups adjacent to the "open" Ti sites, while the Lewis acidity is due to the framework Ti ions. It is the internal silanols in TS-1 that contribute to the condensation of EDA rather than its Lewis acid sites. A small crystal size of TS-1 benefits more the secondary condensation of PIP to TEDA, a bulky reaction which requires open reaction spaces such as pore entrance and external surface, compared to the primary condensation of EDA to PIP.

Acknowledgments

We gratefully acknowledge NSFC of China (20673038, 20873043), Science and Technology Commission of Shanghai Municipality (09XD1401500, 08JC1408700, 07QA14017), 973 Program (2006CB202508), 863 Program (2007AA03Z34), and Shanghai Leading Academic Discipline Project (B409). Y.W. thanks the PhD Program Scholarship Fund of ECNU 2008.

Appendix A. Supplementary material

Supplementary data associated with this article can be found, in the online version, at doi:10.1016/j.jcat.2009.06.016.

References

[1] Ullmann's Encyclopedia of Industrial Chemistry, vol. A2, VCH, 1998, p. 16.
[2] A. Belhekar, T.K. Das, K. Chaudhari, S.G. Hegde, A.J. Chandwadka, Stud. Surf. Sci. Catal. 113 (1998) 195.
[3] H.G. Bosche, K.Baer, K. Schneider, DE Patent 2, 442, 929, 1976.
[4] I. Hudea, M. Biemel Werner, R. Czifra, RO Patent 85, 563, 1984.
[5] G. Engemann, G. Spielberger, US Patent 3, 080, 371, 1963.
[6] N. Srinivas, D. Venu Gopal, B. Srinivas, S.J. Kulkarni, M. Subrahmanyam, Micropor. Mesopor. Mater. 51 (2002) 43.
[7] Y. Bhat, J. Das, S. Ali, B.D. Bhatt, A.B. Halgeri, Appl. Catal. A 148 (1996) L1.
[8] R. Anand, B.S. Rao, Catal. Commun. 3 (2002) 479.
[9] M. Selvaraj, B.R. Min, Y.G. Shul, T.G. Lee, Micropor. Mesopor. Mater. 74 (2004) 157.
[10] M. Frauenkron, B. Stein, US Patent 6, 562, 971 B2, 2003.
[11] G. Bellussi, M.S. Rigguto, Stud. Surf. Sci. Catal. 85 (1994) 177.
[12] B. Notari, Adv. Catal. 41 (1996) 253.
[13] H. Ichihashi, Catal. Catal. (Shyokubai) 47 (2005) 190.
[14] A. Thangaraj, S. Sivasanker, P. Ratnasamy, J. Catal. 137 (1992) 252.
[15] D. Srinivas, R. Srivastava, P. Ratnasamy, Catal. Today 96 (2004) 127.
[16] R.S. Drago, S.C. Dias, J.M. McGilvray, A.L.M.L. Mateus, J. Phys. Chem. B 102 (1998) 1508.
[17] G. Deo, A.M. Turek, I.E. Wachs, Zeolites 13 (1993) 365.
[18] A. Auroux, A. Gervasini, E. Jorda, A. Tuel, Stud. Surf. Sci. Catal. 84 (1994) 653.
[19] R. Srivastava, D. Srinivas, P. Ratnasamy, Catal. Lett. 91 (2003) 133.
[20] J.Q. Zhuang, Z.M. Yan, X.M. Liu, X.C. Liu, X.W. Han, X.H. Bao, U. Mueller, Catal. Lett. 83 (2002) 87.
[21] T. Tatsumi, K.A. Koyano, Y. Shimizu, Appl. Catal. A 200 (2000) 125.
[22] A. Corma, U. Diaz, E.M. Domine, V. Fornés, J. Am. Chem. Soc. 122 (2000) 2804.
[23] P. Wu, T. Komatsu, T. Yashima, J. Phys. Chem. 100 (1996) 10316.
[24] P. Wu, T. Komatsu, T. Yashima, J. Catal. 168 (1997) 400.
[25] M.A. Camblor, A. Corma, A. Martínez, J. Pérez-Pariente, J. Chem. Soc. Chem. Commun. (1992) 589.
[26] P. Wu, T. Tatsumi, T. Komatsu, T. Yashima, J. Phys. Chem. B 105 (2001) 2897.
[27] P. Wu, T. Tatsumi, Catal. Surv. Asia 8 (2004) 137.
[28] A. Tuel, Zeolites 16 (1996) 108.
[29] X.W. Guo, G. Li, X.F. Zhang, X.S. Wang, Stud. Surf. Sci. Catal. 112 (1997) 499.
[30] P.R. Reddy, M. Subrahmanyam, S.J. Kulkarni, Catal. Lett. 54 (1998) 95.
[31] E. Astorino, J.B. Peri, R.J. Willey, G. Busca, J. Catal. 157 (1995) 482.
[32] D. Scarano, A. Zecchina, S. Bordiga, F. Geobaldo, G. Spoto, G. Petrini, G. Leofanti, M. Padovan, G. Tozzola, J. Chem. Soc. Faraday Trans. 89 (1993) 412.
[33] W. Lin, H. Frei, J. Am. Chem. Soc. 124 (2002) 9292.
[34] R. Buzzoni, S. Bordiga, G. Ricchiardi, C. Lamberti, A. Zecchina, G. Bellussi, Langmuir 12 (1996) 930.
[35] C. Pazé, S. Bordiga, C. Lamberti, M. Salvalaggio, A. Zecchina, G. Bellussi, J. Phys. Chem. B 101 (1997) 4740.
[36] F. Bonino, A. Damin, S. Bordiga, C. Lamberti, A. Zecchina, Langmuir 19 (2003) 2155.
[37] C. Ngamcharussrivichai, P. Wu, T. Tatsumi, J. Catal. 235 (2005) 139.
[38] C. Lamberti, S. Bordiga, D. Arduuino, A. Zecchina, F. Geobaldo, G. Spano, F. Genoni, G. Petrini, A. Carati, F. Villain, G. Vlaic, J. Phys. Chem. B 102 (1998) 6382.
[39] G. Yang, X.J. Lan, J.Q. Zhuang, D. Ma, L.J. Zhou, X.C. Liu, X.W. Han, X.H. Bao, Appl. Catal. A 337 (2008) 58.
[40] L. Chen, L. Norena, J. Navarrete, J. Wang, Mater. Chem. Phys. 97 (2006) 236.
[41] J. Anderson, C. Fergusson, I. Rodriguez-Ramos, A. Gueerero-Ruiz, J. Catal. 192 (2000) 344.
[42] C.B. Khouw, M.E. Davis, J. Catal. 151 (1995) 77.
[43] J.W. Ward, Am. Chem. Soc. Monogr. 171 (1979) 118.
[44] E. Dumitriu, V. Hulea, S. Kaliaguine, M.M. Huang, Appl. Catal. A 135 (1996) 57.
[45] H. Bludau, H.G. Karge, W. Niessen, Micropor. Mesopor. Mater. 22 (1998) 297.